Raman Spectral Imaging of a Carbon Nanotube Intramolecular Junction

Stephen K. Doorn,[1,*] Michael J. O'Connell,[1] Lianxi Zheng,[1] Yuntian T. Zhu,[1] Shaoming Huang,[2] and Jie Liu[2]
[1]*Los Alamos National Laboratory, Los Alamos, New Mexico 87545, USA*
[2]*Department of Chemistry, Duke University, Durham, North Carolina 27708, USA*
(Received 20 May 2004; published 3 January 2005)

Confocal Raman spectral imaging results are presented for a metal-to-semiconductor intramolecular junction (IMJ) on an isolated carbon nanotube. Spectra observed at the junction are consistent with the symmetry lowering expected from the occurrence of pentagon-heptagon defects to produce the chirality shift. The IMJ transition zone is sharp and preserves the nanotube diameter. These results have significant implications for the future use of IMJs as electronic devices, including how prevalent these structures are and how their growth may be rationally targeted. Raman imaging has been demonstrated to be a powerful tool for IMJ studies and provides a more accessible method for further studies of IMJ structure and growth.

DOI: 10.1103/PhysRevLett.94.016802 PACS numbers: 73.22.–f, 78.30.–j

The remarkable electronic properties of single wall carbon nanotubes (SWNTs) have been demonstrated to have significant potential for use in nanoscale electronics and field-effect transistor (FET) based logic devices [1,2] and for nanophotonics applications [3]. Of particular interest for device applications are SWNT intramolecular junctions (IMJs) formed through so-called 5–7 defects of pentagon-heptagon structures that allow merging of different chiral nanotube structures to form direct metallic-metallic (M-M), semiconductor-semiconductor (S-S), or metallic-semiconductor (M-S) junctions. Such IMJs are expected to display single nanotube device behavior as diodes, rectifiers, and S-S potential for electro-optics [4–6]. Additionally, such single nanotube devices may eventually replace complex source-drain structures in nanotube FETs. A number of theoretical studies have investigated the topological consequences of the introduction of 5–7 defects to form IMJs and have probed the resulting electronic [7–13] and optical properties [14]. To realize IMJ applications, both methods for controlled growth of these structures and convenient characterization tools must be developed. A number of results suggest that IMJ junctions may be induced in a single nanotube, including experiments demonstrating electric field-induced junction formation [15], heat-induced structural changes [16], and diameter reduction through *e*-beam irradiation [17]. These junctions can also occur naturally in nanotubes synthesized in common production processes. Indirect evidence for these structures has been provided by observations of bent geometries [5,18] and transport measurements along the nanotube length [5,19]. Recently, direct STM imaging and density of states measurements have provided the best direct evidence for the occurrence of IMJs [20,21]. Optical spectroscopic probes for IMJs may provide a faster and more accessible means for detection and structural characterization of IMJs, yet no reports of optical IMJ studies have appeared to date.

We present results from confocal Raman imaging of individual ultralong chemical vapor deposition (CVD) produced carbon nanotubes. We observed a chiral shift along the length of an individual nanotube and are able to spectrally image the region over which this chiral transition takes place. Spectral evolution over this transition region provides an indication of the structural changes required to change chirality. The observed spectra are consistent with a structural change from semiconductor to metallic character to form an M-S junction. This junction appears to form within the spatial resolution of our measurements, with minor structural changes continuing into longer length scales (μm). These results represent the first optical and vibrational characterization of a nanotube IMJ and demonstrate Raman imaging as a powerful, nondestructive, and more accessible tool than STM for detection and characterization of these structures. Moreover, Raman measurements are not limited to nanotubes grown on conductive surfaces, allowing IMJ studies for nanotubes grown on a broad range of substrate types. It will be an important method for guiding future efforts at targeted synthesis of IMJ materials.

Single nanotube Raman spectroscopy has been demonstrated to be a powerful technique for electronic and structural characterization of short nanotubes ($< 1\ \mu$m) and small bundles [22]. Single nanotube sensitivity is possible due to the large density of states accessed with resonance excitation, allowing high quality spectra to be obtained with no other enhancement mechanisms being required. Recent reports of near-field [23] and confocal [24,25] Raman imaging on individual short nanotubes has demonstrated that single-tube Raman sensitivity can allow spectroscopic mapping of nanotube structural details. Recent advances in CVD growth of ultralong nanotubes [26,27] has resulted in mm to cm long nanotubes that are interesting systems on which structural evolution can be examined over large length scales. Raman mapping over hundreds of microns and even for whole nanotube lengths on these novel structures will potentially allow a more general and accessible means for large-scale screening for, and characterization of, IMJs than is feasible with STM probing.

 © 2005 The American Physical Society

The carbon nanotubes in this study were grown by the rapid heating catalytic CVD method [26,27] with methane as the carbon source and Fe/Mo as the catalyst. Briefly, an Fe/Mo carbonyl complex [28] solution is applied to a silicon (with 600 nm SiO_2) wafer. The Si wafer is introduced into a quartz tube, followed by heating at 650 °C for 5 min in a hydrogen atmosphere. The Si wafer was then moved away from the tube center and a methane hydrogen mixture (850 sccm CH_4/400 sccm H_2) was introduced into the reactor while heating the tube to 900 °C. The Si wafer was quickly transferred into the center area of the tube. The growth lasted for 30 min, and was stopped by switching the gas mixture to argon and cooling the furnace to room temperature. An SEM image of the resultant nanotubes is shown in Fig. 1. The region along the left edge (where the catalyst has been applied) contains a dense growth of short intertwined nanotubes. Well separated, individual long nanotubes extend to the right of the catalyst region, ranging in length from a few hundred microns to 3 mm for the longest nanotube. The isolated nature of individual long nanotubes allows Raman measurements to be performed free of the intertube interactions present in the STM IMJ studies [20,21].

Raman spectra and images were obtained with 514.5 nm excitation through a confocal imaging Raman microscope. Spectra at each image point are the average of two 4 s integrations acquired with 6 mW excitation through a 100 ×, 0.9 NA (numerical aperture) objective. The excitation spot size was 1 μm, as confirmed by a line profile obtained across the nanotube perpendicular to its length. As the spot size is much larger than the nanotube diameter, ultimate spatial resolution is determined by the nanotube itself. Single nanotube resolution is obtainable due to the large spatial separations (typically at least 10 μm) between the long nanotubes found in our sample.

Raman spectra were sampled along the length (every 50 μm, for a total of 725 μm) of the longest nanotube shown in Fig. 1. For most of the sampled length, the observed G-peak spectra were similar to that shown in Fig. 2(a), with only minor changes in frequency ($\sim$ 1 cm^{-1}) and relative intensity between the G_+ and G_- peaks (at 1601 and 1582 cm^{-1}, respectively). No radial breathing mode (RBM) was observed in these spectra, indicating that the 514.5 nm excitation wavelength was outside the resonant window of this nanotube's electronic transitions. Enhancement of the G peak in this case results from resonance of the Raman scattered photon with a lower lying electronic transition [29]. Additionally, the D peak was also absent (as found for the other 19 long tubes sampled), indicating relatively low levels of defect sites present in these nanotubes. At a point near 640 μm along the sampled length the nanotube spectrum was found to change to that shown in Fig. 2(e), with G_+ and G_- peaks at 1594 and 1576 cm^{-1}, respectively. In addition to the dramatically altered G peak, a RBM at 147 cm^{-1} now appears. The absence of the D band continues in this region. This spectrum remains stable over the remaining 85 μm probed. A Raman image of the transition region over which this spectral change occurs (circled region in Fig. 1) is shown in Fig. 2.

The spectral evolution shown in Fig. 2 is consistent with a change in chirality from a semiconducting to a metallic nanotube. The G-peak spectrum of Fig. 2(a) has a Lorentzian line shape, consistent with this location being a semiconducting nanotube. The spectrum in Fig. 2(e), however, has the Breit-Wigner-Fano line shape characteristic of metallic nanotubes [22]. Given the 1 μm spatial resolution of the Raman imaging, it is reasonable to question whether the imaged region is due to a single nanotube

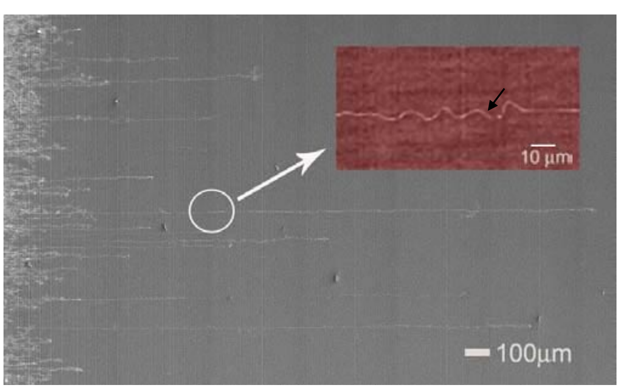

FIG. 1 (color online). SEM image of the ultralong nanotube sample used for Raman imaging investigations. Raman mapping was performed on the longest nanotube in the image. The circled highlight and inset is the transition region over which the M-S IMJ occurs (marked by the black arrow in the inset).

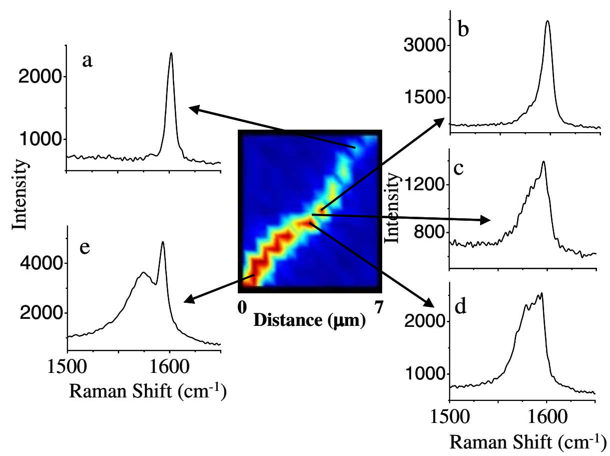

FIG. 2 (color online). Raman spectral image of IMJ transition (note that the image is flipped horizontally with respect to the SEM image). Image intensity is of the G-peak region integrated from 1500–1650 cm^{-1}. Spectra for each image point were obtained at 0.5 μm intervals. Individual spectra across this transition region show (a) the semiconductor region, (b)–(d) the central transition regions, and (e) the metallic region.

with an IMJ transition, or is it just two different nanotubes resting side by side. If the data are from two nanotubes, the spectra in the overlapping region would be expected to simply be the sum of the G-peak spectra from the different nanotube types. This, however, is not the case [30]. Additionally, atomic force microscopy (AFM) imaging of the transition region shows that only one nanotube exists in the imaged region and that no separate nanotubes are found to branch into this region along the 90 μm imaged via AFM [30]. Finally, spectra are also obtained far from the tip of the nanotube, where the catalyst particle is located, the only location in these ultralong nanotubes where multiple tubes might be expected to exist.

Besides providing evidence for an M-S junction, the individual Raman image spectra can yield information on the junction structural transformation. A RBM at 147 cm^{-1} is observed for the metallic nanotube [Fig. 3(a)], indicating a diameter of 1.69 nm [22]. Although the RBM loses intensity across the transition region, it is still weakly present at nearly the same frequency in the initial semiconductor spectra (see also Ref. [30]). The 19 cm^{-1} separation between the semiconductor G_+ and G_- peaks also gives an approximation [22] of its diameter as $1.6(\pm 0.2)$ nm. These results indicate that the nanotube likely maintains its diameter across the IMJ transition. IMJs previously imaged by STM demonstrate that these can occur through structural rearrangement that

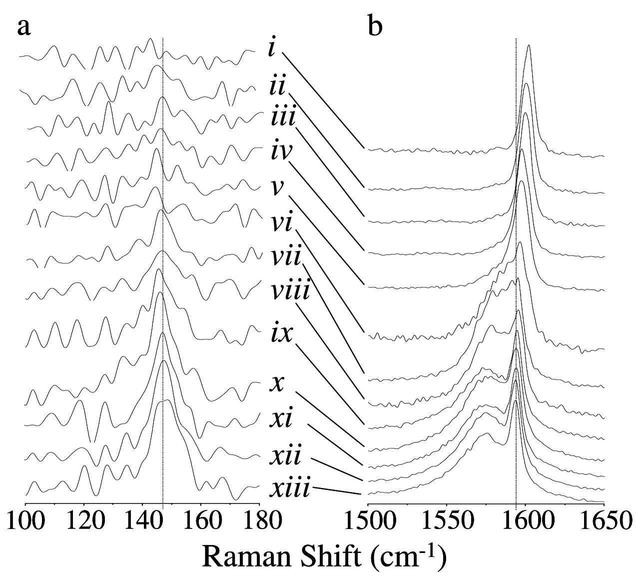

FIG. 3. Evolution of (a) the radial breathing mode and (b) the G-peak region spectra across the length of the transition region. Spectra from top to bottom correspond to individual points along the nanotube image shown in Fig. 2, from upper right (semiconductor) to lower left (metallic) at the following distances: (i) 1.1 μm; (ii) 2.8 μm; (iii) 3.5 μm; (iv) 4.4 μm; (v) 5.3 μm; (vi) 5.7 μm; (vii) 6.2 μm; (viii) 7.5 μm; (ix) 8.4 μm; (x) 8.9 μm; (xi) 9.3 μm; (xii) 9.8 μm; and (xiii) 10.2 μm. The IMJ occurs at approximately 6 μm.

results in a significant change in diameter across the transition region [20,21]. In contrast, the IMJ imaged here occurs with a minimal change in diameter. Although the diameter appears to remain stable, minor changes (an increase of 4 cm^{-1}) in the G-mode frequency for several microns into the semiconductor region [Fig. 3(b)] indicate that some minor structural "relaxation" (or rearrangement) to produce the final stable semiconductor region continues to occur [21]. The metallic G peak, however, retains a stable frequency up to the transition region itself.

As is observed, when resonance enhancement is present for the metallic RBM, the electronic transition energy for a semiconductor of the same diameter places it off resonance with the same excitation wavelength. The lack of resonance between the excitation wavelength and semiconductor transitions is also consistent with the generally lower G-peak intensities for the semiconductor segment, compared to the metallic.

The broad, weakly structured G-peak spectra observed at the IMJ transition region [see Figs. 2(b)–2(d) and 3(b)] indicate a lowering of nanotube symmetry during the transition. Geometric modeling of the nanotube structure [20,21] has demonstrated that the M-S transition can occur through incorporation of multiple 5–7 defect pairs in the transition region. The presence of these defects results in a decreased nanotube symmetry, consistent with our observations. Throughout the imaged IMJ region of Fig. 2, the nanotube defect band (the D peak, commonly observed near 1340 cm^{-1}) is very weak and unobservable [30]. The extreme weakness of this defect peak indicates that the 5–7 defects occur over only a very narrow distance—within the spatial resolution of our imaging. Although minor changes in G-peak frequencies occur on longer length scales, the bulk of the IMJ transition appears to occur within our imaging resolution. The evolution of the Raman spectra across the transition region thus contains significant information pertaining to the structural changes occurring to produce an M-S IMJ. Detailed modeling of the nanotube geometric and electronic structural transition to reproduce the observed Raman data will be the subject of future efforts and will result in a complete picture of the IMJ structural transition for comparison with models developed from STM data [20,21].

The observation of an IMJ in these new ultralong nanotubes has important implications for their use as electronic devices. A major question in this regard: How prevalent are these structures? If they are infrequent, then, in general, these nanotube types will display one continuous chirality, with uniform device properties. Nanotube annealing might be used to remove or convert the few tubes that contain IMJs. We observe an IMJ occurrence only once in 20 nanotubes probed. STM probing of ~100 nanotubes has shown that occurrence frequencies can be as high as 10% in laser oven-grown samples [20]. Clearly, more extensive probing of these ultralong nanotube types to obtain better occurrence statistics will be important. If IMJs are found to be a generally occurring phenomenon, however, then the quick heating CVD growth method could be an important means for rational synthesis of IMJs. Thus, Raman imaging will be an important tool for understanding and steering growth parameters for optimized rational control of large-scale IMJ production. Raman imaging will also be an important technique for developing a better understanding of nanotube nucleation, growth, and termination mechanisms in general. It will provide a sensitive structural probe for detailed characterization and modeling of IMJs and other structural defect types that will aid in developing a better understanding of variations in electronic structure and transport properties through defect or junction sites. As such, confocal Raman imaging of single ultralong nanotubes will be a very versatile new tool for characterizing structures over large length scales, providing a powerful, and potentially more versatile, complement to near-field optical and STM imaging techniques.

This work has been supported by LANL LDRD funding. M. O'C. acknowledges the support of the Director of Central Intelligence. Efforts at Duke University are supported by Office of Naval Research Grant No. N00014-04-1-0765 issued to Rice University with a subagreement to Duke University.

*To whom all correspondence should be addressed.
Electronic address: skdoorn@lanl.gov

[1] P. Avouris, Acc. Chem. Res. **35**, 1026 (2002).
[2] A. Bachtold *et al.*, Physica (Amsterdam) **16E**, 42 (2003).
[3] J. A. Misewich *et al.*, Science **300**, 783 (2003).
[4] P. L. McEuen, Nature (London) **393**, 15 (1998).
[5] Z. Yao *et al.*, Nature (London) **402**, 273 (1999).
[6] R. H. Baughman, A. A. Zakhidov, and W. A. de Heer, Science **297**, 787 (2002).
[7] B. I. Dunlap, Phys. Rev. B **49**, 5643 (1994).
[8] Ph. Lambin *et al.*, Chem. Phys. Lett. **245**, 85 (1995).
[9] J.-C. Charlier, T. W. Ebbesen, and Ph. Lambin, Phys. Rev. B **53**, 11 108 (1996).
[10] L. Chico *et al.*, Phys. Rev. Lett. **76**, 971 (1996).
[11] R. Saito, G. Dresselhaus, and M. S. Dresselhaus, Phys. Rev. B **53**, 2044 (1996).
[12] V. Meunier, P. Senet, and Ph. Lambin, Phys. Rev. B **60**, 7792 (1999).
[13] M. S. Ferreira *et al.*, Phys. Rev. B **62**, 16 040 (2000).
[14] W. Fa, X. Yang, J. Chen, and J. Dong, Phys. Lett. A **323**, 122 (2004).
[15] G. W. Ho, A. T. S. Wee, and J. Lin, Appl. Phys. Lett. **79**, 260 (2001).
[16] M. Yudasaka *et al.*, Carbon **41**, 1273 (2003).
[17] S. B. Chikkannanavar *et al.* (to be published).
[18] J. Han *et al.*, Phys. Rev. B **57**, 14 983 (1998).
[19] P. G. Collins *et al.*, Science **278**, 100 (1997).
[20] M. Ouyang *et al.*, Science **291**, 97 (2001).
[21] H. Kim *et al.*, Phys. Rev. Lett. **90**, 216107 (2003).
[22] M. S. Dresselhaus *et al.*, Carbon **40**, 2043 (2002).
[23] A. Hartschuh *et al.*, Phys. Rev. Lett. **90**, 095503 (2003).
[24] C. Jiang *et al.*, J. Phys. Chem. B **107**, 8742 (2003).
[25] V. G. Hadjiev *et al.*, Nanotechnology **15**, 562 (2004).
[26] S. Huang *et al.*, Adv. Mater. **15**, 1651 (2003).
[27] S. Huang, X. Cai, and J. Liu, J. Am. Chem. Soc. **125**, 5636 (2003).
[28] Y. Li *et al.*, Chem. Mater. **13**, 1008 (2001).
[29] A. Jorio *et al.*, Phys. Rev. B **65**, 155412 (2002).
[30] See EPAPS document E-PRLTAO-94-123502 for *D*-peak spectra, for the RBM frequency plot, and for *G*-peak modeling and AFM data supporting the observation that only one nanotube is imaged in the IMJ region. A direct link to this document may be found in the online article's HTML reference section. The document may also be reached via the EPAPS homepage (http://www.aip.org/pubservs/epaps.html) or from ftp.aip.org in the directory /epaps/. See the EPAPS homepage for more information.